N65-89023
~~X64-10993~~ *
Code 2A
29p
(NASA TM X-51126)

TESTING EXPERIENCE AND CALIBRATION EXPERIMENTS IN A MACH NUMBER 12, 1-FOOT HYPERSONIC ARC TUNNEL

W. B. Boatright, R. B. Stewart, and D. I. Sebacher

[1964] 29p refs

Co-auth.: NASA Langley Research Center
Langley Station, ~~Hampton~~, Va.

For presentation ~~Presented~~ at the ~~Third~~ 3rd Hypervelocity Techniques Symposium

Denver, ~~Colorado~~
March 17-18, 1964

~~Limited~~
~~Users Only~~

TESTING EXPERIENCE AND CALIBRATION EXPERIMENTS IN A MACH NUMBER 12, 1-FOOT HYPERSONIC ARC TUNNEL

W. B. Boatright,* R. B. Stewart,* and D. I. Sebacher*

NASA Langley Research Center
Langley Station, Hampton, Va.

ABSTRACT

10993

A hypersonic arc-heated wind tunnel with a 1.5-megawatt arc heater, a 1-foot-diameter test section, and a 5-stage steam ejector for a vacuum is described. The rotating-arc heater geometry is described and modifications which have been made to the heater to improve its efficiency and contamination level are discussed. Pitot pressure calibration experiments show that the Mach number in the test section varies only from about 11.85 to 12.1 over a 9-inch length, in spite of the fact that a conical nozzle is used. Wall static pressure measurements indicate that the flow is near chemical equilibrium. Data with a long nozzle extension and a large variation in back pressure show that feedback through the tunnel boundary layer did not invalidate the wall static pressure data. An electron beam apparatus which permits measurements of the free-stream density, and the vibrational and rotational temperature is discussed and results are presented.

AUTHOR

INTRODUCTION

At several locations throughout the country, efforts are being directed toward the application of the arc heater for increasing the Mach number range of conventional hypersonic tunnels, or toward creating a real-gas environment where hypersonic aerodynamic investigations can be made with air chemistry effects present. Facilities of this type with test times in the order of minutes are particularly suited to certain types of hypersonic testing. For example, with long test times the measurement of low static pressures is easier. Also tests involving the aerodynamics associated with mass transfer cooling may be undertaken more readily. This paper will discuss some of the arc-heater development work that has been conducted and some calibration and testing experience that has been obtained for the most part in a hypersonic arc-heated tunnel with a Mach number 12, 1-foot-diameter test section. Many of the results will be directly applicable to testing and data interpretation in a larger 10-megawatt arc-heated facility, which is in the final construction stage at the Langley Research Center. This larger facility, called the Hyperthermal Leg of

*Aerospace Engineer.

Available to [illegible] and NASA Center Only

the Hypersonic Aerothermal Dynamics Facility will have a 4-foot-diameter test section and will exhaust into a 100-foot-diameter vacuum sphere.

NOMENCLATURE

A	nozzle cross-sectional area
A^*	throat cross-sectional area
B	magnetic flux density
d^*	nozzle throat diameter
H_t	tunnel stagnation enthalpy
I	radiation intensity
J	current
M	Mach number
p_1	wall static pressure
$p_{t,1}$	tunnel stagnation pressure
$p_{t,2}$	stagnation pressure behind a normal shock
T_t	stagnation temperature

Subscripts:

(0-1) (1-0) (1-1) (1-2)	nitrogen vibrational bands (see appendix)

TUNNEL

The 1-foot hypersonic arc tunnel has a 1.5-megawatt arc heater. The heater was designed to use existing motor-generator apparatus for the d-c power supply. The heater exhausts through a 1/8-inch-diameter throat, a 5° half-angle conical nozzle, a cylindrical test section 1-foot in diameter, and a straight pipe diffuser, to a 5-stage steam ejector. The steam ejector will provide a back pressure of 100 microns at a tunnel mass flow of 0.03 lb/sec. Using only about 900 kw of the available power, the tunnel has been operated at stagnation pressures of 12 to 25 atm and at stagnation enthalpies of 1,500 to 3,000 Btu/lb. The enthalpy

capability is not inversely proportional to the stagnation pressure within this stagnation-pressure range since the efficiency increases with stagnation pressure. Figure 1(a) shows a photograph of the heater and figure 1(b) shows a view of a portion of the conical nozzle, the test section, and part of the diffuser. The instrumentation in the foreground of figure 1(b) and the apparatus directly beneath the test section were used in an electron beam experiment to be described subsequently and are part of a special test.

ARC HEATER

A sketch of the arc-heater configuration presently in use with this tunnel is shown in figure 2. It is a design which provides a clean, uncontaminated airstream and is suited for high-pressure operation. The previously quoted stagnation-pressure range of the tunnel is limited by the mass flow capability of the steam ejector and not by the pressure capability of the arc heater.

The distinguishing feature of this type of heater is the high magnetic field strength which is used to rotate the arc. Field strengths of 12,000 to 15,000 gauss are present in the region of the arc. The resulting $J \times B$ force rotates the arc at a very high speed. In fact, from tests on a similar heater being operated at the Langley Research Center, there is evidence that the arc is a diffused disk rather than a filament (ref. 1). More details of the heater design used with the 1-foot hypersonic arc tunnel can be found in reference 2.

An arc heater of this general design excels in its ability to produce a clean airstream and to operate at high pressures. One of its shortcomings is that at low air mass flow rates, it is not as efficient as some of the other designs presently in use throughout the country. Much higher efficiencies are usually quoted for heater designs which use a geometry such that the arc is parallel to the airflow and which force the arc through a constrictor. One of the reasons for the relatively poor efficiency of the heater shown in figure 2, when it is attached to the 1-foot hypersonic arc tunnel, is the small throat size. The experimental points shown in figure 3 represent a series of tests performed by Mr. Roger B. Stewart at the Langley Research Center wherein the heater shown in figure 2 was exhausted into a water-cooled calorimeter. The main purpose of these tests was to evaluate various techniques for enthalpy determination and three different throat sizes were used; however, the trend of increasing efficiency with increasing air mass flow through the heater is clearly evident in figure 3. The test points shown in figure 3 represent power inputs to the arc from about 380 kw to 430 kw. With the exception of the results denoted by the diamond symbols, the stagnation

pressures were from 200 to 380 psia. The results represented by the diamond symbols were tested at stagnation pressures from 110 to 165 psia.

In an effort to improve the efficiency of this heater a number of modifications have been made. Using silver-plated electrodes instead of oxygen-free copper appeared to be advantageous from the standpoint of decreasing contamination, but a negligible increase in efficiency was observed.

Silver plating has its problems also, since imperfect plating can cause a burnout. During testing, several burnouts were surmised to have been caused by the fact that when a tiny bubble in the plated silver was heated, a small piece of silver would flake off the electrode and the metallic vapor would evidently cause the arc to dwell in this area.

One modification which resulted in an increase in efficiency is illustrated in figure 4. Changing the center electrode configuration from that shown in the lower part of the photograph to that shown in the upper part, resulted in a large increase in efficiency and enthalpy capability. Only that portion of the center electrodes to the left of the white, boron nitride pieces in figure 4 protrude into the arc chamber so only this portion is significant in changing the performance of the heater. The main difference between the two electrodes is that the copper electrode in figure 4 is aerodynamically cleaner. Consequently the flow of air in the region of the arc is less turbulent. Operating at a stagnation pressure of about 150 psi and the same power input, the enthalpy of the exhausted air was increased from about 2,000 Btu/lb to about 3,000 Btu/lb when using the improved center electrode. The half-filled diamond symbols in figure 3 denote test points taken with the improved center electrode configuration shown in the upper part of figure 4, and indicate the increased efficiency that was obtained.

TUNNEL FLOW CALIBRATION

Pitot Pressures

The testing experience in this arc-heated facility up to the present has emphasized stream calibration experiments. Figure 5(a) shows the Mach number distribution along the tunnel center line and figure 5(b) shows a cross-stream pitot survey. The stream Mach number is about 12, and the facility has a test core about 5 inches in diameter. Figure 5(a) shows that over a longitudinal distance of about 9 inches, the Mach number varies only from 11.85 to 12.1 at the noted stagnation conditions. This compares favorably with the gradient in some contoured nozzles. The shallow Mach number gradient is of course due to the fact that the tunnel wall boundary layer builds up at the proper rate so as to cancel the Mach number gradient which is produced by an inviscid conical expansion. This type of closed test

section, with a pressure rise at the juncture of the conical nozzle and cylindrical test section, very likely contributes to the fact that the Mach number is so uniform in this region. These results would not be expected at widely varying stagnation conditions. In fact, experiments in helium wind tunnels with similar nozzle geometry, colder flow, and stagnation pressures of 1,000 to 3,000 psi have not realized as shallow a gradient as is shown in figure 5(a) (ref. 3).

Chemical State of Nozzle Flow

A serious problem connected with the development of high enthalpy, hypersonic wind tunnels is concerned with the possibility of nonequilibrium flow in the nozzle. An investigation which was conducted in a forerunner of the present 1-foot arc tunnel produced some encouraging results concerning the problem of avoiding nozzle nonequilibrium flow. The small tunnel in which this experiment was conducted was identical to the present 1-foot arc tunnel except the conical nozzle only extended from the 1/8-inch throat to a 3-inch-diameter test section. Later, an extension to this investigation was conducted in the 1-foot arc tunnel.

The basic experiment will be reported in reference 4; it consisted of measuring wall static pressures along the nozzle from the 1/8-inch throat to the 3-inch-diameter test section. Pitot pressure measurements were also made along the center line of the nozzle at corresponding locations. In order to match the pitot pressure measurement to a given wall orifice location it was assumed that conical source flow existed in the nozzle. This technique of using wall static pressures to define the flow has its limitations; it was pursued after other techniques such as measurements of static pressures on half-wedges and slender, pointed probes proved too complicated as a result of the induced pressure effects on the small size probes required in the 3-inch-diameter nozzle. Successful measurements using probes have, however, been made in larger nozzles. For example, the shock tunnel experiments of reference 5 showed the degree of equilibrium in the nozzle of a shock tunnel over a wide range of stagnation conditions.

A plot of the wall static pressure against pitot pressure, measured at various locations down the nozzle is shown in figure 6. Both the static and pitot pressure measurements are nondimensionalized by dividing by the tunnel stagnation pressure. Pitot pressure is insensitive to whether the flow is in equilibrium or frozen, and the results are plotted in this manner simply to circumvent the difficulty connected with determining the variation in static pressure with effective nozzle area ratio.

Also shown in figure 6 are the calculated variations of pitot and static pressure down the conical nozzle for different stagnation conditions and for different assumptions concerning the degree of equilibrium of the flow. The nonequilibrium prediction was computed by the method of reference 6, which considers only a 3-component gas mixture (N_2, O_2, and O). At these relatively low enthalpies, however, it is close to the more accurate prediction of reference 7. A comparison of the experimental and calculated results shown in figure 6, indicates that the nozzle flow is very close to equilibrium for nozzle locations down to a 3-inch diameter.

One of the objections to the use of wall static pressures to indicate the variation of static pressure down a nozzle is the possibility of a high-pressure feedback upstream through the tunnel wall boundary layer. This would raise the wall static pressures, and if the flow were partially frozen it would move the experimental points toward the equilibrium curve. The results shown in figure 7 indicate that this effect was insignificant. The circular symbols represent the variation of the nozzle wall static pressure with geometric area ratio for the tests conducted in the small arc-heated tunnel with its 3-inch-diameter test section. This corresponds to configuration 2 in figure 7. The back pressure for these tests was about 0.34 psia. The square symbols are the data obtained at the same orifice locations but with a conical extension which provided a test section 1 foot in diameter (configuration 1). The back pressure when using this nozzle was about 0.003 psia. The fact that the pressures presented in figure 7 check so closely for the widely varying back pressure indicates that the data shown in figure 6 are not significantly affected by a high-pressure feedback upstream through the tunnel boundary layer. Repeat measurements of the wall static pressure with the pitot tube at different longitudinal locations down the nozzle also showed that, within the range tested, the pitot tube had little effect on those wall static pressures upstream of the pitot tube location.

Electron Beam Experiments

Since a high Mach number hypersonic tunnel usually has test section densities that are rather low, the electron beam appears attractive as a research tool for defining the static properties in the test section. The method is particularly suitable in that the beam has a negligible effect on the flow, and point measurements can be obtained in the flow. The technique for interpreting the measurements has been previously developed in observations of the aurora borealis and have been applied to a low density facility by E. P. Muntz, reference 8. Mr. D. I. Sebacher and Mr. R. J. Duckett built the electron beam generator and made the measurements to be reported in this paper.

The electron beam is collimated across the test section of the tunnel and the light from the molecular ion N_2^+ is observed spectroscopically. From the distribution of light intensity in the bands, the rotational and vibrational temperature can be computed. The theory which applies to this operation is discussed in the appendix. Also from the intensity of the beam as compared to a bench calibration at the same beam current, the free-stream density can be determined.

Details of the construction of the electron beam generator and a schematic diagram of its electrical circuit is shown in figure 8. The electron beam generator is shown in cross section as it appeared when attached to the bottom of the tunnel test section. The upper part of figure 8 denotes the test section window through which the beam could be viewed. As part of the auxiliary apparatus, a vacuum pump is needed to evacuate the chamber in which the filament and accelerating orifice plates are located. The pressure in this chamber should be about 5×10^{-5} mm Hg.

Although the magnetic coil of the arc heater was located about 6 feet from the tunnel test section and the electron beam generator, it was necessary to magnetically shield the generator. The shield is not shown in figure 1(b) or figure 8. It was only necessary to shield the region of the electron beam generator near the filament, since only in this region where the velocity of the electrons is relatively low is there an appreciable deflection of the beam due to the magnetic field.

The results of the vibrational temperature measurements using the electron beam technique are shown in figure 9. The solid curves were calculated using the technique discussed in the appendix. The predicted variation of the light intensity ratio for two bands of N_2^+ is shown by these curves. Thus, a measurement of the intensity ratio, when used in conjunction with the curves for these molecular bands, will determine the vibrational temperature of the nitrogen in the free stream. The experimental measurements shown by the shaded area in figure 9 were taken from a scan of the spectrum presented in figure 10. When using a direct read-out on the spectrometer, there are some accuracy difficulties as discussed in the appendix, so these measurements should be considered preliminary. However, it is encouraging that the results using the two different band systems indicate about the same vibrational temperature in the free stream. This indicated vibrational temperature of about 1,500° K is higher than that which would be predicted for equilibrium flow. For the measured tunnel stagnation pressure of 19.4 atm and the measured stagnation enthalpy of 1,935 Btu/lb, the free-stream static temperature (assuming equilibrium flow) should be about 150° K. At the

nozzle location where the diameter is 3 inches and where pressure measurements indicated that the flow was in chemical equilibrium, the equilibrium static temperature should be about 470° K. The vibrational temperature measurements at the 1-foot section using the electron beam technique indicate a temperature which is even higher than this temperature. It thus appears that the flow is not in vibrational equilibrium.

A discussion of the relative relaxation times of the vibrational energy mode and the chemical dissociation is given in reference 9. The estimate given in reference 9 indicates that at about 4,000° K, the oxygen recombination reaction time and the vibrational relaxation time are about the same. Later experimental evidence obtained in shock tube measurements of the dissociation rate have indicated rates slower than that predicted by reference 9.

A comparison of the results of the wall static pressure measurements and the electron beam measurements presented in this paper does not necessarily indicate that chemical recombination rates are faster than vibrational relaxation rates. If the flow were frozen chemically at a temperature of 1,500° to 2,000° K, the amount of energy involved in dissociation would be so small that nonequilibrium effects would not be detectable by the pressure measurements.

The reliability of these vibrational temperature measurements will be significantly improved when direct read-out is not used but a spectrogram is taken. It is expected that rotational temperature will also be obtained from this spectrogram using the method discussed in the appendix and illustration in figure 11. Rotational temperature could not be obtained with the direct read-out attachment on the spectrometer because the individual rotational lines in a band could not be resolved.

The use of the electron beam to determine the free-stream density proved straightforward. Further details of this technique are given in the appendix. Within the operating range of the tunnel, the calibration curve was only slightly nonlinear. The measured value of the density in the tunnel test section was 0.25×10^{-6} slugs per cu ft. The calculated value, assuming equilibrium flow in the nozzle, was 0.22×10^{-6}.

CONCLUSIONS

Testing experience in a small arc-heated, hypersonic wind tunnel has indicated the following conclusions:

1. The arc-heater design used with the 1-foot, hypersonic arc tunnel provides an especially clean and uncontaminated airstream and is suited for high pressure, high mass flow rates, and relatively

high power operation. However, at low air mass flow rates, this type of heater might not be as efficient as other types.

2. For the stagnation pressure and enthalpy range at which the 1-foot arc tunnel is being operated, a surprisingly uniform flow exists in the test section in spite of the fact that the nozzle is conical. Indications are that the closed test section type of design used for this wind tunnel is contributing to the favorable, viscous contouring of the nozzle.

3. Wall static pressure measurements in the conical nozzle have indicated that the flow is in chemical equilibrium over at least the first 1/4 of the nozzle length. These measurements were made at stagnation pressures from 12 to 20 atm and at enthalpy levels of about 2,000 Btu/lb. A nozzle extension experiment indicated that the wall static pressures were not significantly affected by feedback upstream through the tunnel wall boundary layer.

4. Preliminary measurements using an electron beam and a direct read-out spectrometer to determine the vibrational temperature indicated that the vibrational temperature of the nitrogen molecules in the airstream is too high to be considered in equilibrium. Rotational temperature measurements could not be obtained with the direct read-out spectrometer but they are expected to be obtained from a spectrogram. The electron beam technique also proved useful for making measurements of the free-stream density in the test section.

APPENDIX

INTERPRETATION OF SPECTROGRAPH MEASUREMENTS USING AN ELECTRON BEAM

D. I. Sebacher

NOMENCLATURE

A	Einstein's spontaneous transition probability
B_v	rotational constant of v vibrational level
C	constant
c	speed of light
F	constant
$G_o(v)$	term values for vibrational levels
h	Planck's constant
I	intensity of radiation
J	rotational quantum number, with electron spin
K	rotational quantum number, with no electron spin
k	Boltzmann constant
N	number of particles
$N_2^+ \; B \; ^2\Sigma$	upper electronic state of nitrogen ion N_2^+
$N_2^+ \; X \; ^2\Sigma$	ground state of nitrogen ion N_2^+
$N_2 \; X \; ^1\Sigma$	ground state of nitrogen molecule
N_o	number of $N_2 \; X \; ^1\Sigma$ molecules
n	number density
Q_r	rotational state sum
Q_v	vibrational state sum
R	gas constant
R_e	electronic transition moment
$R_{v'v_2''}$	transition moment
$\left\|R_{v'v_2''}\right\|^2$	transition probability
r	internuclear distance

T	temperature
ν	wave number
σ	collision diameter
ψ	eigenfunctions

Subscripts:

v	vibrational
1	designates the state $N_2\ X\ ^1\Sigma$
2	designates the state $N_2^+\ X\ ^2\Sigma$

Superscripts:

'	indicates upper state in transition
"	indicates lower state in transition

GENERAL CONSIDERATIONS

To use the electron beam technique, a narrow column of electrons (10 to 20 kv) is passed normal to the flow through the test section. These electrons excite a small number of the particles making up the flow and the resulting emission of light from the excited particles is observed spectrographically to determine the vibration and rotation temperatures and the number density of the species observed.

In air, the light observed is dominated by the first negative system of N_2^+ and has been proven by Muntz (ref. 8) to follow, according to the Franck-Condon Principle, the excitation and emission paths as shown in the opposite sketch.

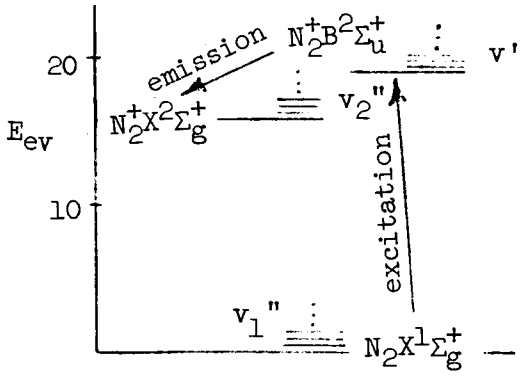

$$N_2\ X\ ^1\Sigma_g^+ \xrightarrow{\text{excitation}} N_2^+\ B\ ^2\Sigma_u^+ \xrightarrow{\text{emission}} N_2^+\ X\ ^2\Sigma_g^+ \qquad (1)$$

Since absolute intensities of the emitted light are difficult to measure, relative measurements are used throughout. To determine the vibrational temperature, the ratios of the relative intensities of various vibrational bands are compared as a function of temperature. To determine the rotational temperature, the variation of the relative intensities of the rotational lines in a vibration band with the rotational quantum number is observed as a function of temperature. To

determine the number density, the relative intensity of the total light of the first negative system is calibrated as a function of density for a given electron beam current. A theoretical description of these measurements is as follows.

VIBRATION TEMPERATURE MEASUREMENTS

The intensity of a spectral line in emission is defined (ref. 10) for the bands under study as

$$I_{em_{v',v_2''}} = N_{v'} hc\nu_{v',v_2''} A_{v',v_2''} \tag{2}$$

where

$$A_{v',v_2''} = \frac{64\pi^4 \nu_{v',v_2''}^3}{3h} \left|R_{v',v_2''}\right|^2 \tag{3}$$

is the Einstein spontaneous emission probability. The transition probability of emission is given by

$$\left|R_{v',v_2''}\right|^2 = \bar{R}_e^2 \left(\int \psi_{v'} \psi_{v_2''} \, dr\right)^2 \tag{4}$$

The number of particles in the v' state is given by

$$N_{v'} = \frac{N_o}{Q_v} \sum_{v_1''} \left(e^{-G_{o_{v_1''}} \frac{hc}{kT}} B_{v',v_1''}\right) \tag{5}$$

where the Einstein transition probability of absorption is given by

$$B_{v',v_1''} = \frac{8\pi^3}{3h^2 c} \left|R_{v',v_1''}\right|^2 \tag{6}$$

and the transition probability of absorption by

$$\left|R_{v',v_1''}\right|^2 = \bar{R}_e^2 \left(\int \psi_{v',v_2''} \, dr\right)^2 \tag{7}$$

Combining these terms in equation (2) then gives

$$I_{em_{v'v_2''}} = \frac{N_o}{Q_v} \sum_{v_1''} \left(e^{-G_{o_{v_1''}} \frac{hc}{kT}} \frac{8\pi^3}{3h^2c} \left| R_{v'v_1''} \right|^2 \right) \left(hc\nu_{v'v_2''} \frac{64\pi^4 \nu^3_{v'v_2''}}{3h} \left| R_{v'v_2''} \right|^2 \right) \tag{8}$$

or

$$I_{em_{v'v_2''}} = D\nu^4_{v'v_2''} \left| R_{v'v_2''} \right|^2 \sum_{v_1''} \left(e^{-G_{o_{v_1''}} \frac{hc}{kT}} \left| R_{v_1'v_1''} \right|^2 \right) \tag{9}$$

where

$$D = \frac{N_o}{Q_v} \left(\frac{8\pi^3}{3h^2c} \right) \left(\frac{64\pi^4}{3h} \right) hc \tag{10}$$

and the ratio of any two bands such as the $(0,1)$ to the $(1,2)$ first negative bands of N_2^+ is given by

$$\frac{I_{(0,1)}}{I_{(1,2)}} = \frac{\nu^4_{(0,1)}}{\nu^4_{(1,2)}} \frac{\left| R_{(0,1)} \right|^2}{\left| R_{(1,2)} \right|^2} \sum_{v_1''=0,1,2\ldots} \left[\frac{e^{-G_{o_{v_1''}} \frac{hc}{kT}} \left| R_{v_0'v_1''} \right|^2}{e^{-G_{o_{v_1''}} \frac{hc}{kT}} \left| R_{v_1'v_1''} \right|^2} \right] \tag{11}$$

The intensity ratios of two bands of the first negative band of N_2^+ were computed as a function of temperature and are shown in figure 9. The relative populations of the vibrational levels of N_2 $X\,{}^1\Sigma$ for various temperatures assuming a Boltzmann distribution can be found in Muntz (ref. 8), and the probabilities and wavelengths used in equation (11) can be found in Bates (ref. 11).

When the electron beam method was applied to the tunnel measurements it was found that the light level of the beam excited emission was so low for the running time of the tunnel that photoelectric techniques were best suited to obtain data. The instrument used was a 3.5-meter Jarrell Ash Spectrometer with a direct read-out attachment using a 1P28 photomultiplier tube. The slit of the spectrograph was removed. A scan of the spectrum during a test is shown in figure 10 with the bands of interest designated. A continuous

background in the visible wavelength is also evident. This background of visible light is probably due to contamination of the stream by copper from the electrodes. The contamination level is believed to be below 0.2 percent; however, because of the sensitivity of the photomultiplier tube even this low contamination level shows on the scan of the spectrum. To the naked eye this background illumination is barely detectable in a darkened room. The vibration temperature computed from the spectrographic scan is shown in the shaded area of figure 9 and is in the range of $1,500^{\circ}$ K. This indicates that the vibration is far out of equilibrium with the static temperature (150° K). The intensities used for this measurement were the integrated intensity under the curve of figure 10 for the bands of interest. It should be noted that at these high temperatures the bands begin to overlap as the higher rotational quantum states become more populated and introduce some uncertainty in the measurements. For this reason, the temperature measurement which is shown should only be considered as an approximate value and the result is therefore shown as a shaded area.

This value of the vibrational temperature should be considered a preliminary measurement. More accurate data will be obtained from a spectrographic plate. The plate will have to be exposed to a series of tests with the tunnel parameters held constant in order to obtain the proper exposure. Because of cooling water limitations, the tests are limited to a duration of about 3 minutes and it appears that an exposure of about 20 minutes is needed to obtain a good spectrographic plate. The resolution provided by the plate with a 100-micron entrance slit will not only give accurate vibrational ratios but will also resolve the rotational structure so that the rotational temperature can be computed.

ROTATIONAL TEMPERATURE MEASUREMENTS

The intensity of the lines of rotation in emission is given by Hertzberg (ref. 10) as

$$I = \frac{C\nu^4}{Q_r}(J' + J'' + 1)e^{-\frac{B'J'(J'+1)hc}{kT}} \tag{12}$$

For a $^2\Sigma_u - {}^2\Sigma_g$ transition as in the case of the first negative bands of N_2^+ and at relatively low temperatures the equation simplifies to

$$I = FK'e^{-\frac{BK'(K'+1)hc}{kT}} \tag{13}$$

If $\ln \frac{I}{K'}$ is plotted against $K'(K' + 1)$, the slope of the straight line gives $\frac{Bhc}{kT}$ from which the rotational temperature T can be computed.

A family of curves of $\ln \frac{I}{K'}$ against $K'(K' + 1)$ as a function of temperature is presented in figure 11 along with some experimental points taken under static conditions at 300° K to check the accuracy of the electron beam method in determining rotational temperatures. An attempt was made to determine the rotational temperature using the direct read-out by obtaining the intensity of the unresolved R branch of the (0,0) band, but the noise-to-signal ratio was too great at the beam light level. Spectrographic plates will be used in the future to determine the rotational structure.

NUMBER DENSITY AS A FUNCTION OF INTENSITY

The emission intensity as a function of the number density is given by Muntz (ref. 8) as

$$I = \frac{nhc\nu_{nm}}{1 + \frac{2n\sigma^2\sqrt{4\pi RT}}{A_{nm}}} \tag{13}$$

Since most of the light due to the electron beam comes from the (0,0) band, the intensity of this band was observed as a function of density and it was found to be fairly linear up to 100 microns of Hg for a 12.5-kv beam.

In actual practice the intensity is calibrated as a function of density before and after each run and the intensity of the beam during the run is then applied to this curve to obtain the stream density during the run.

REFERENCES

1. Mayo, Robert F., and Davis, Don D., Jr.: Magnetically Diffused Radial Electric-Arc Air Heater Employing Water-Cooled Copper Electrodes. [Preprint] 2453-62, American Rocket Society, Mar. 1962.

2. Boatright, William B., Stewart, Roger B., and Grimaud, John E.: Description and Preliminary Calibration Tests of a Small Arc-Heated Hypersonic Wind Tunnel. NASA TN D-1377, 1962.

3. Johnston, Patrick J., and Snyder, Curtis D.: Static Longitudinal Stability and Performance of Several Ballistic Spacecraft Configurations in Helium at a Mach Number of 24.5. NASA TN D-1379, 1962.

4. Stewart, Roger B., and Grimaud, John E.: Flow Evaluation in a Samll Arc-Heated Hypersonic Wind Tunnel. NASA Proposed TN. (File No. L-3334.)

5. Nagamatsu, H. T., Workman, J. B., and Sheer, R. E., Jr.: Hypersonic Nozzle Exapnsion of Air With Atom Recombination Present. Jour. of Aero/Space Sci., 1961, 28(11), 833-837.

6. Glowacki, W. J.: Effect of Finite Oxygen Recombination Rate on the Flow Conditions in Hypersonic Nozzles. Aeroballistic Research Report No. 148, Naval Ordnance Lab., White Oak, Maryland.

7. Eschenroeder, Alan Q., Boyer, D. W., and Hall, J. G.: Exact Solution for Nonequilibrium Expansions of Air With Coupled Chemical Reactions. Cornell Aeronautical Lab. Rept. No. AF 1413-A-1, AFOSR Contract No. AF 49-638-792, May 1961.

8. Muntz, E. P.: Measurement of Rotational Temperature, Vibrational Temperature, and Molecule Concentration in Non-Radiating Flows of Low Density Nitrogen. UTIA Rep. No. 71, Apr. 1961.

9. Heims, Steve P.: Effect of Oxygen Recombination on One-Dimensional Flow at High Mach Numbers. NASA TN 4144, 1958.

10. Hertzberg, G.: Molecular Spectra and Molecular Structure. D. Van Nostrand Co., Princeton, New Jersey, 1950.

11. Bates, D. R.: The Intensity Distribution in the Nitrogen Band Systems Emitted From the Earth's Upper Atmosphere. Proc. Royal Soc. A196,217, 1949.

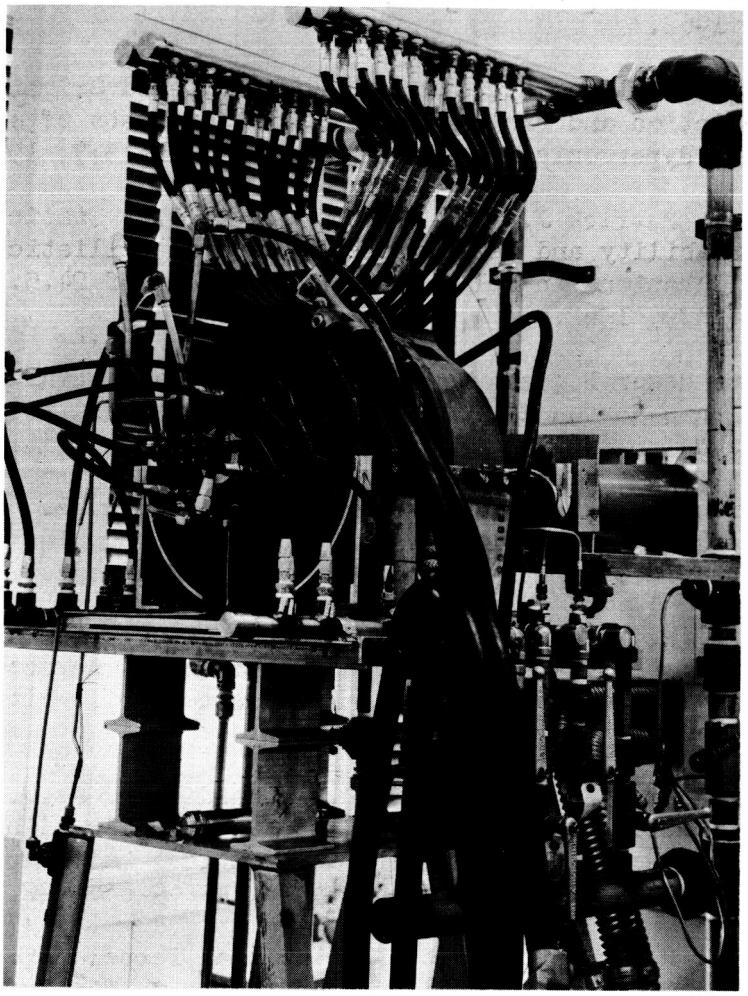

NASA
L-63-691

(a) Arc-heater portion of tunnel. (Center electrode removed.)

Figure 1.- Photograph of 1-foot hypersonic arc tunnel.

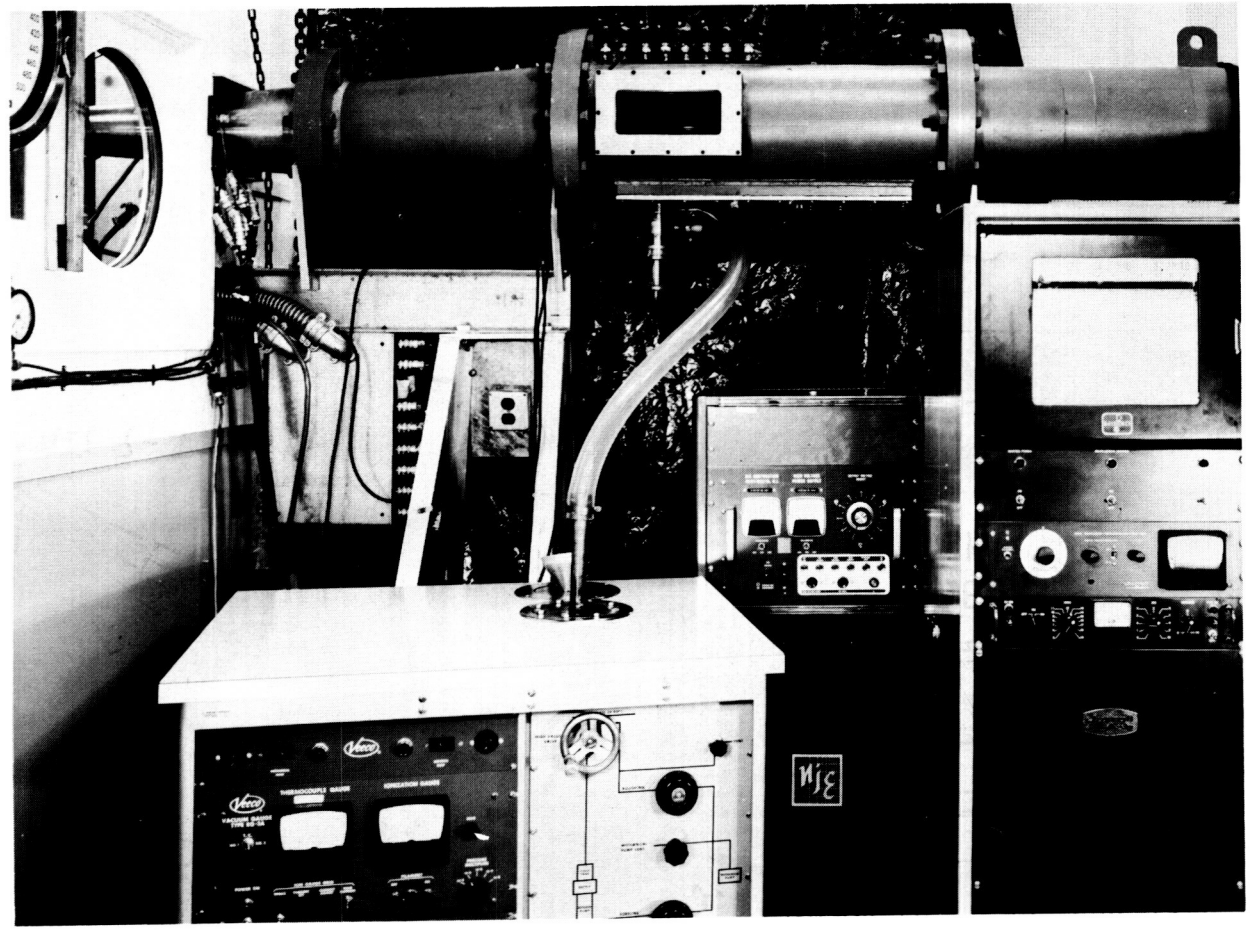

NASA
L-63-8136

(b) Conical nozzle, test section, and diffuser portion of tunnel.

Figure 1.- Concluded.

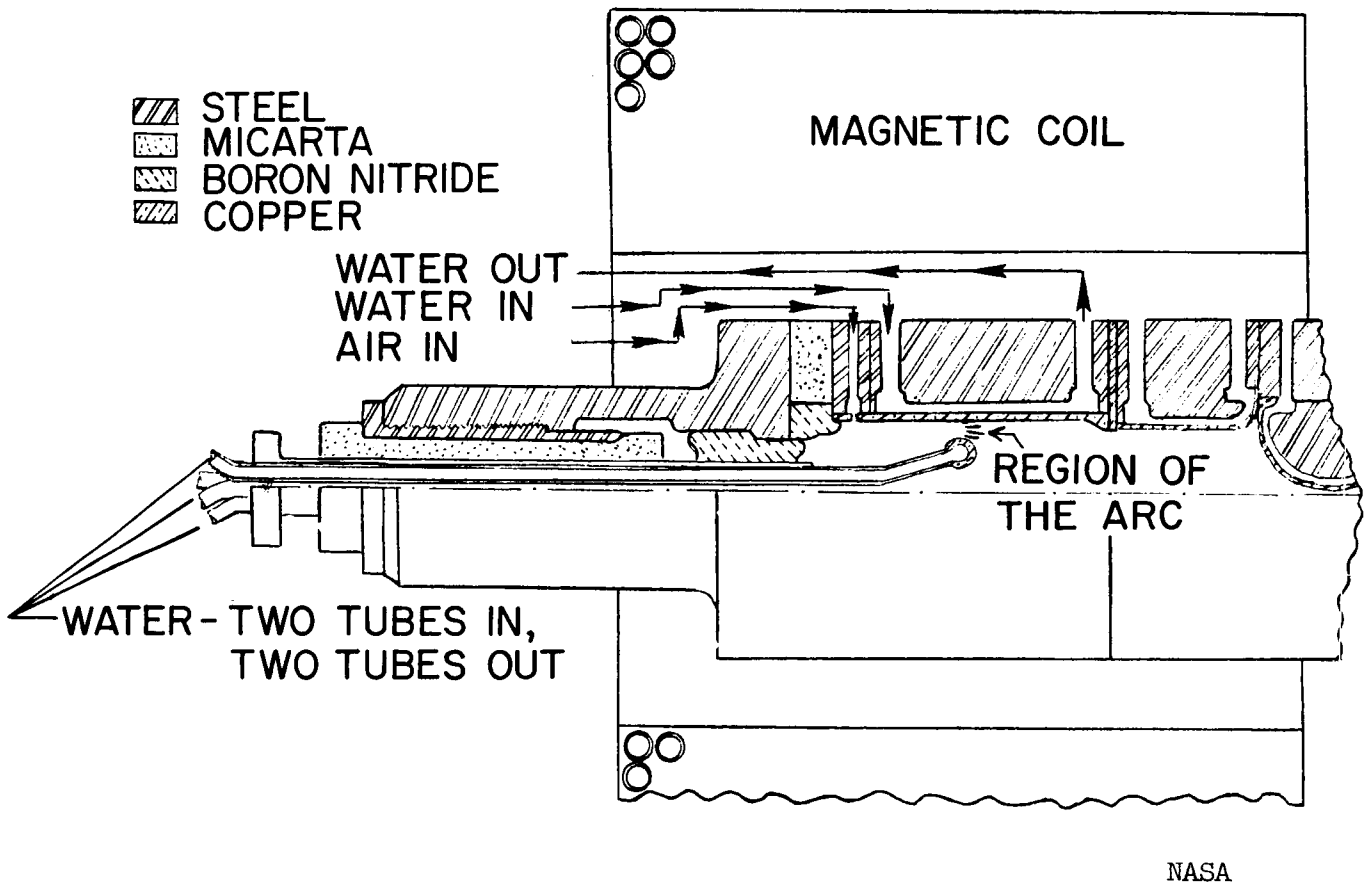

Figure 2.- Sketch of arc-heater configuration.

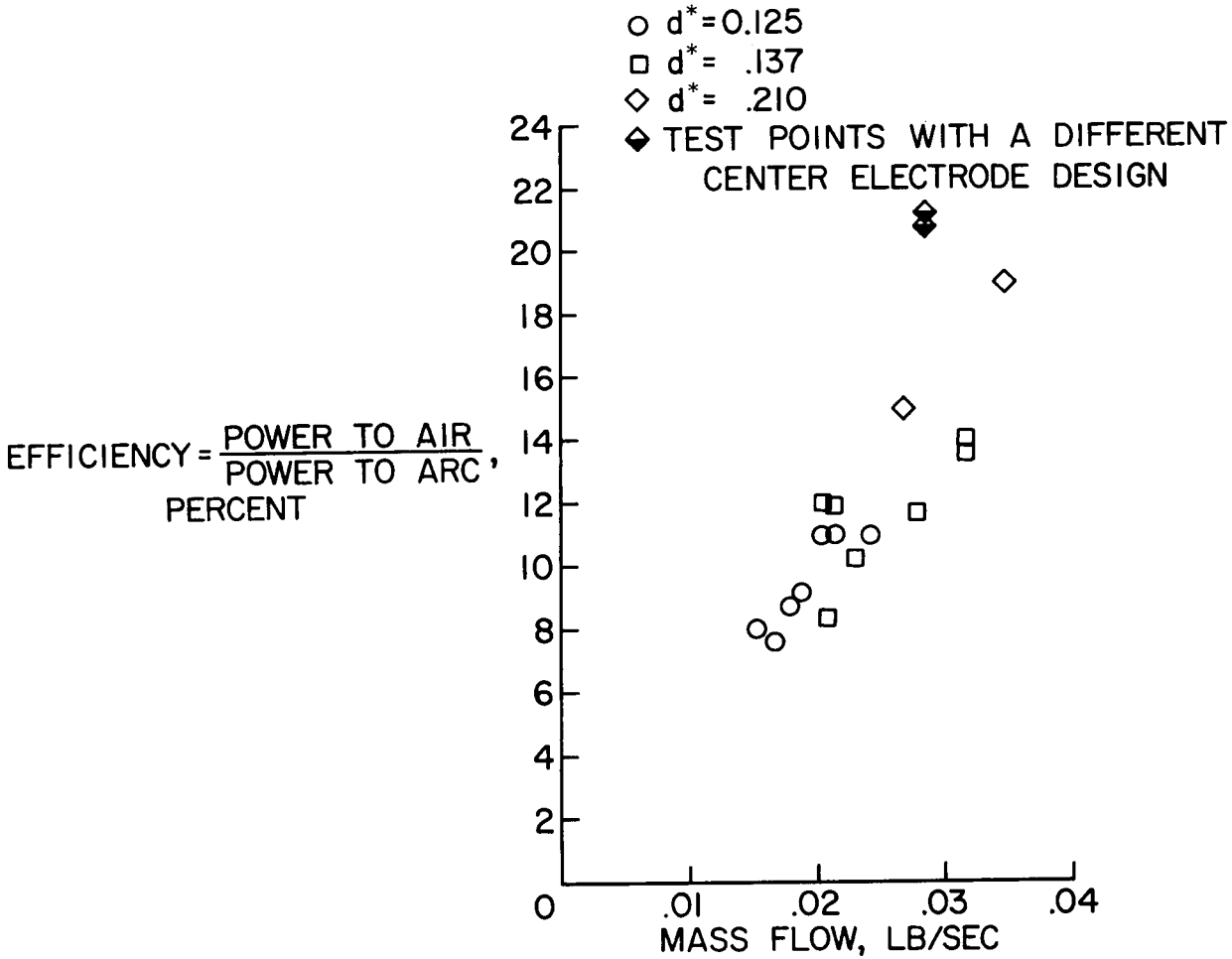

Figure 3.- Arc-heater efficiency as a function of air mass flow through the heater.

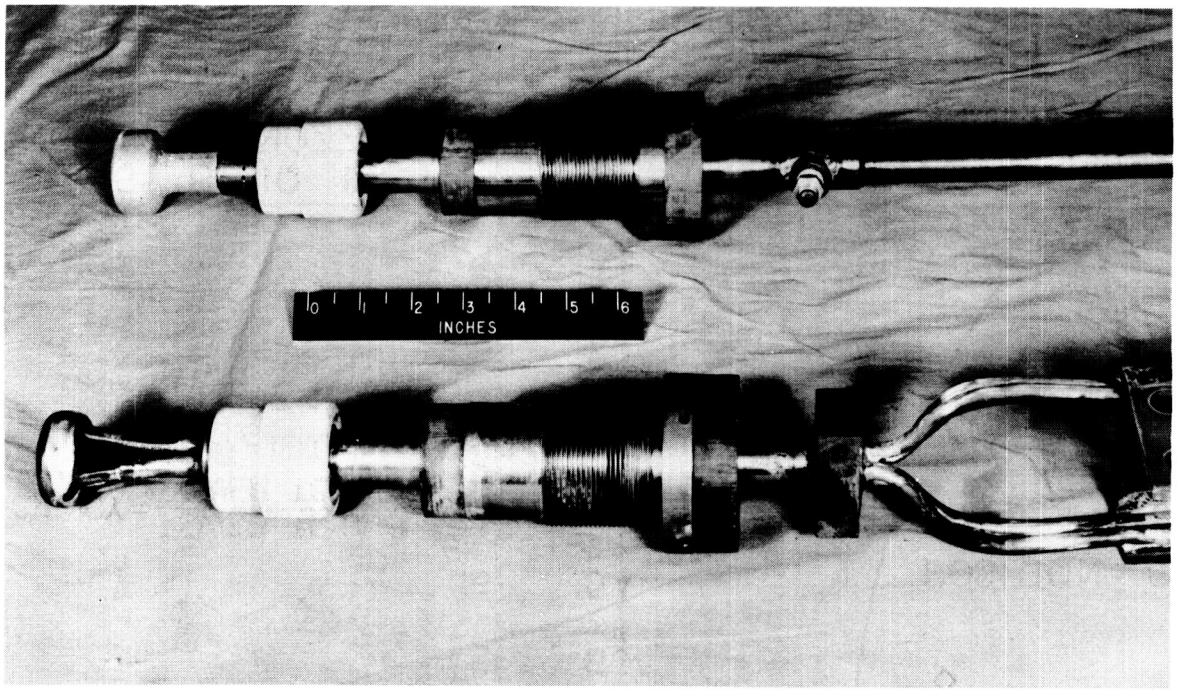

NASA
L-63-8137

Figure 4.- Center electrode configurations.

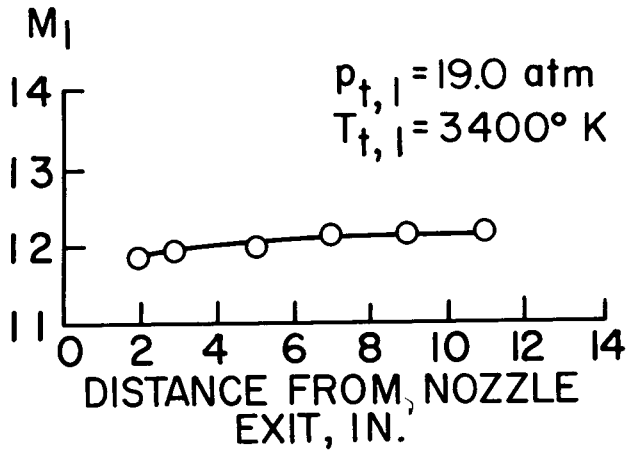

(a) Mach number distribution along center line of test section. (Station 0 is at juncture of conical nozzle and cylindrical test section.)

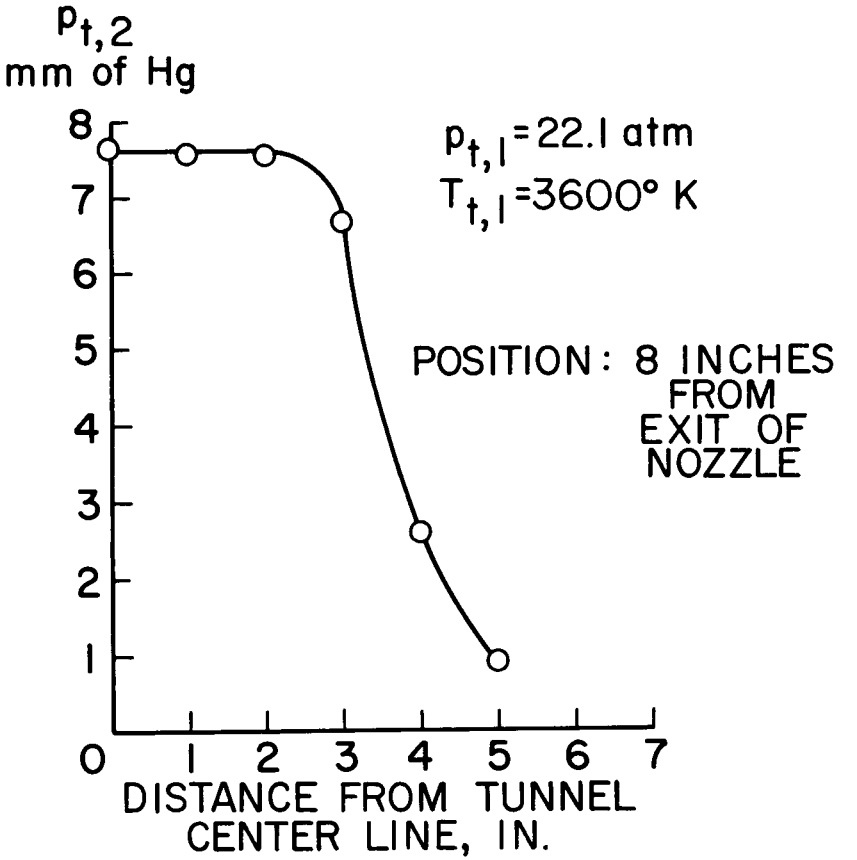

(b) Lateral pitot survey.

NASA

Figure 5.- Flow surveys in 1-foot hypersonic arc tunnel.

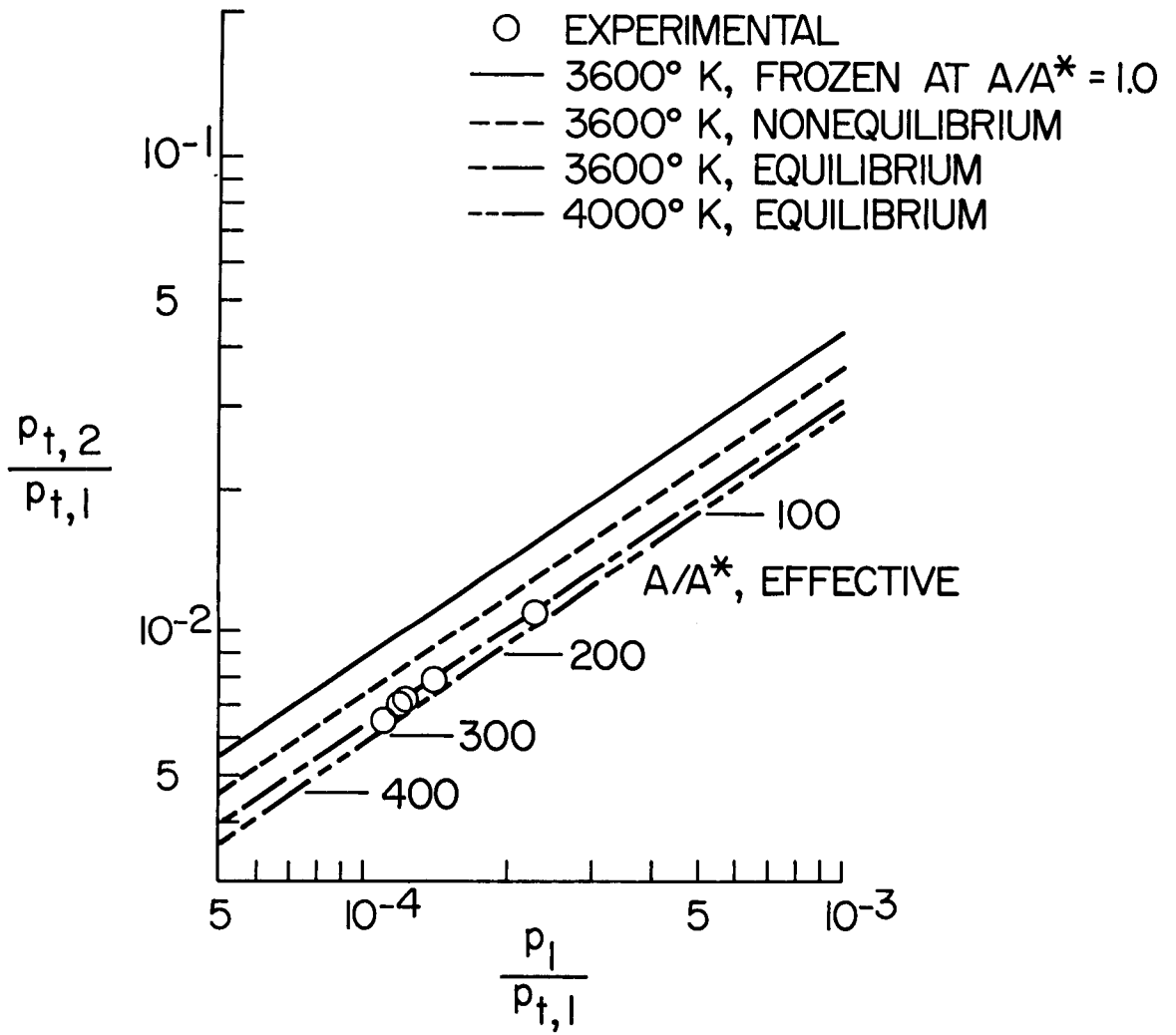

NASA

Figure 6.- Measured and calculated pitot pressure variation with wall static pressure.

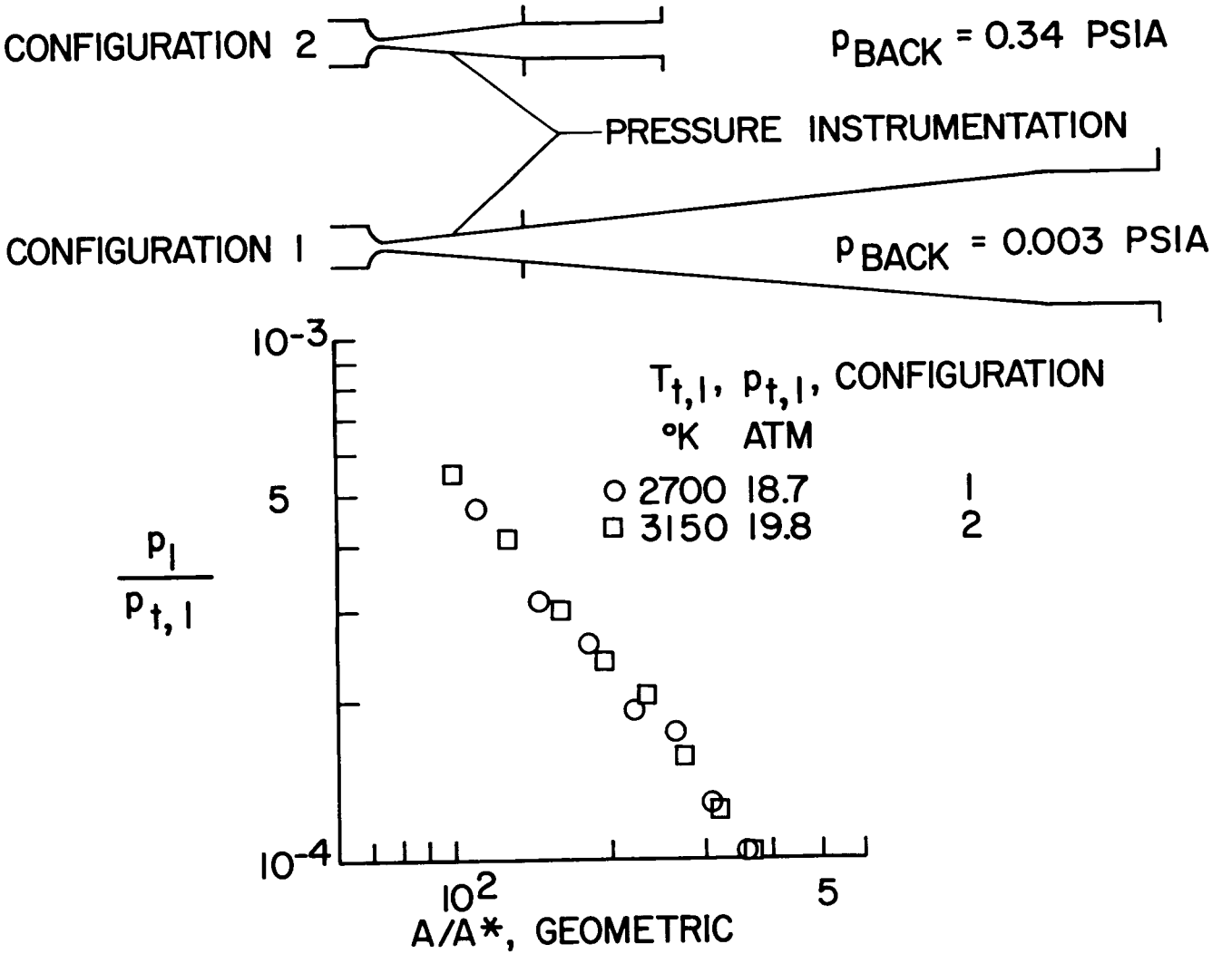

Figure 7.- Wall static pressure profiles for different tunnel back pressures.

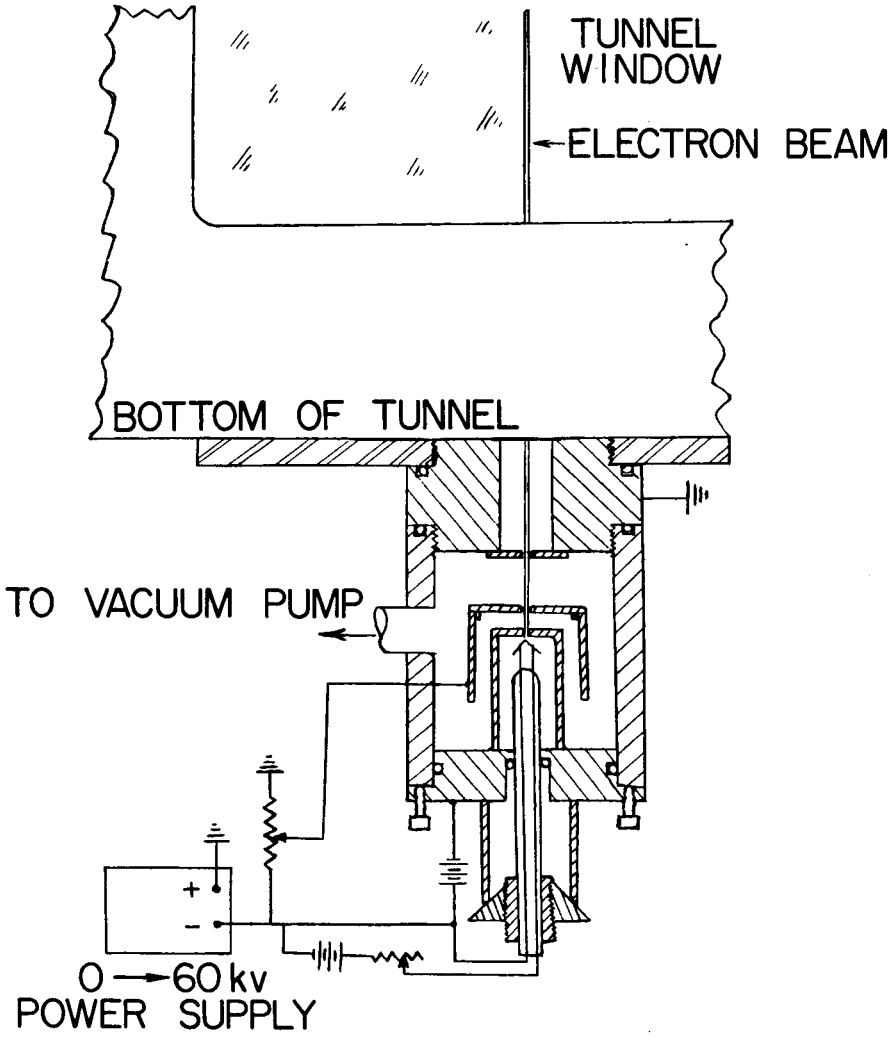

NASA

Figure 8.- Electron beam generator attached to tunnel.

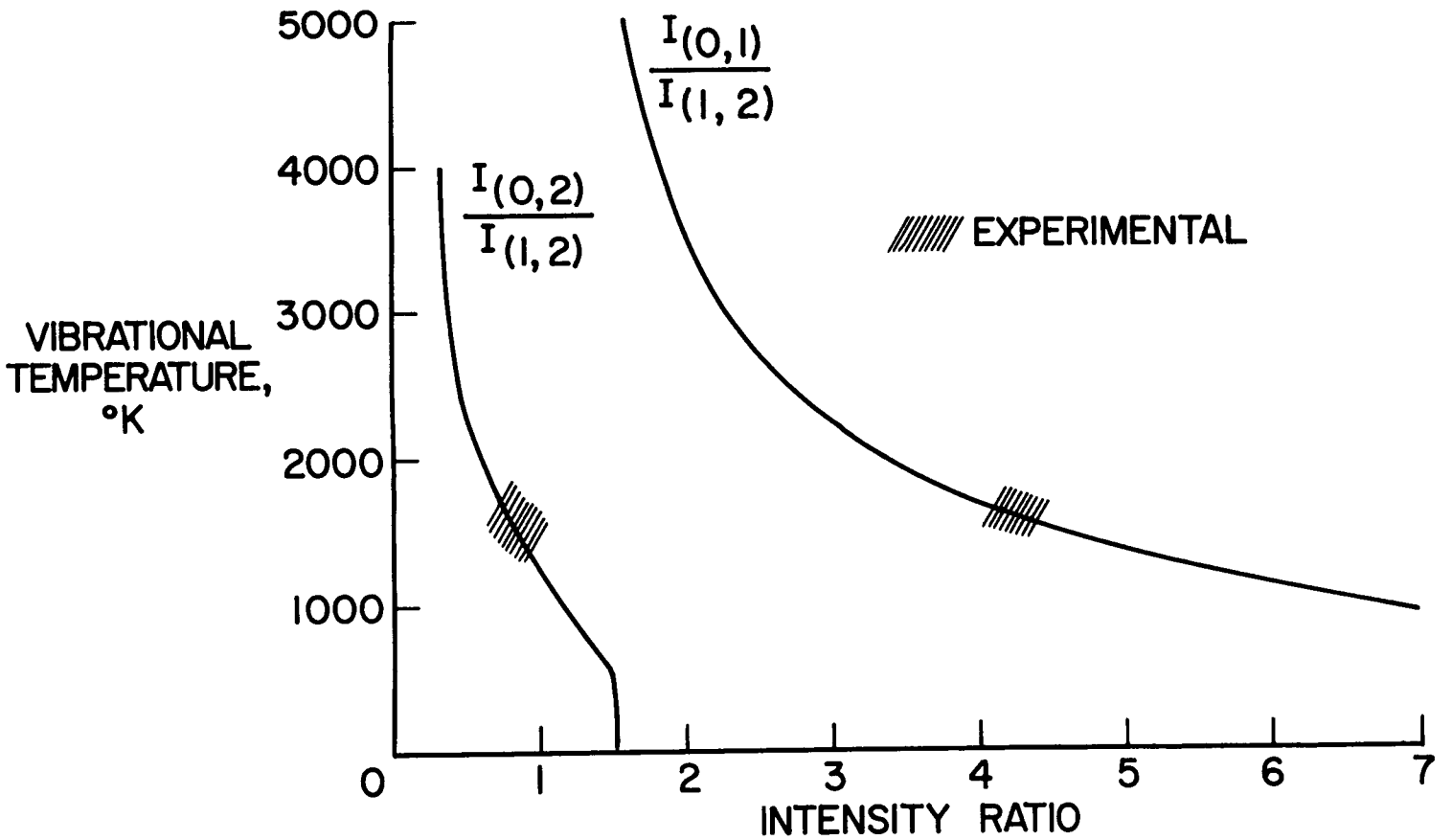

Figure 9.- Vibrational temperatures as a function of band intensity ratio.

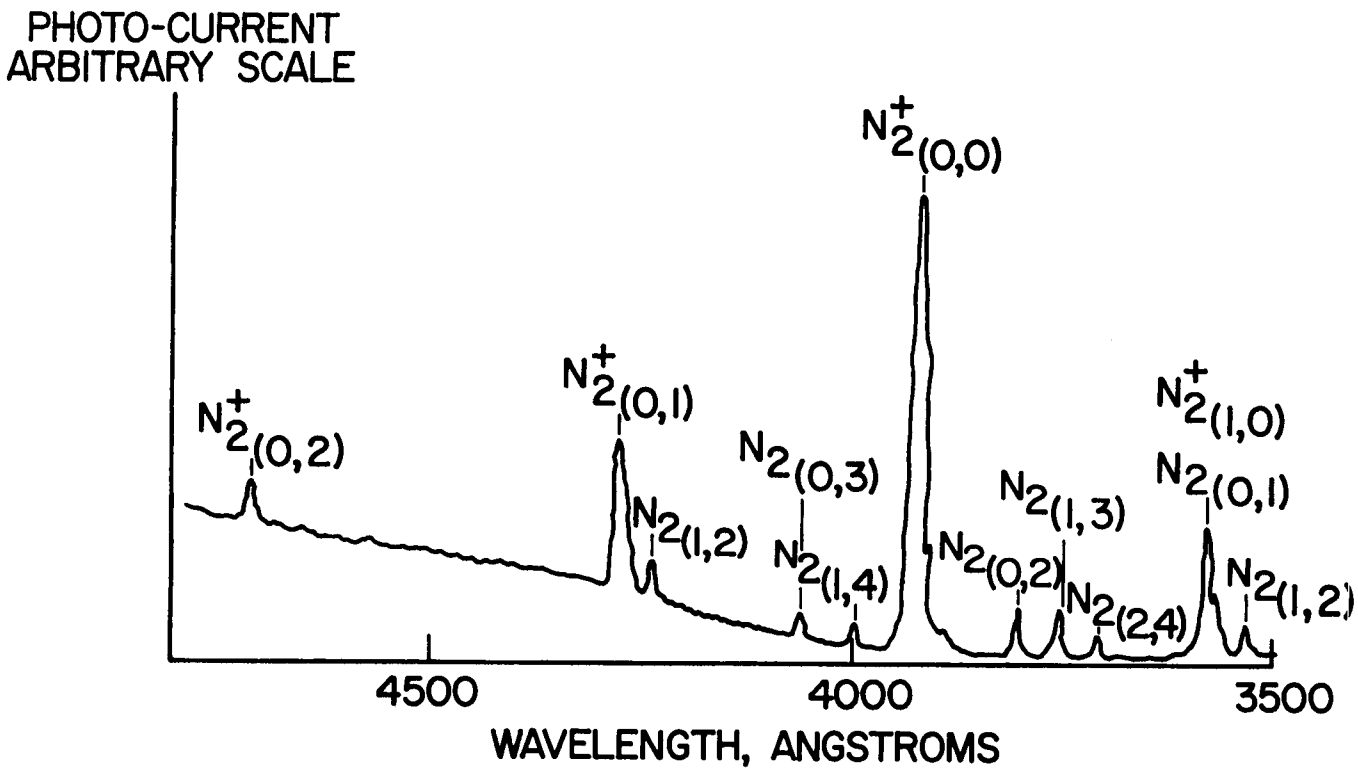

NASA

Figure 10.- Emission spectrum observed during a test as measured by direct read-out attachment on spectrograph.

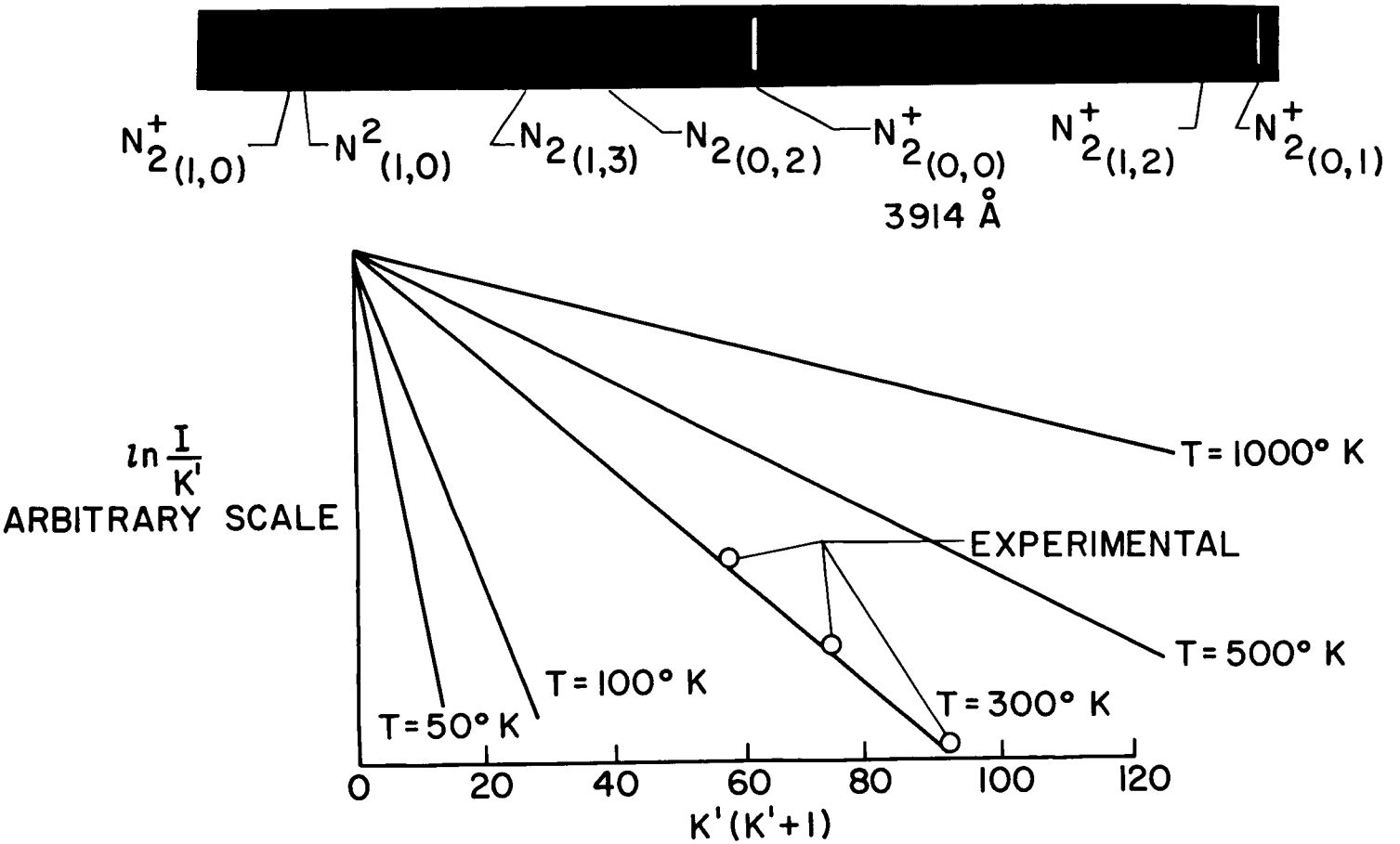

NASA

Figure 11.- Curves of $\ln \frac{I}{K'}$ against $K'(K' + 1)$ as a function of rotational temperature for the R branch of the (0,0) band of N_2^+. Also shown are experimental points determined from the spectrum above under static conditions at 300° K to check the accuracy of the method.

NASA-Langley, 1963